Earthquakes and Structures, *Vol. 17, No. 1 (2019) 75-89*
DOI: https://doi.org/10.12989/eas.2019.17.1.075

Seismic performance of RC frame having low strength concrete: Experimental and numerical studies

Muhammad Rizwan[a], Naveed Ahmad[*] and Akhtar Naeem Khan[b]

Earthquake Engineering Center, Department of Civil Engineering, UET Peshawar, 25120 Khyber Pakhtunkhwa, Pakistan

(Received April 29, 2018, Revised April 6, 2019, Accepted May 17, 2019)

Abstract. The paper presents experimental and numerical studies carried out on low-rise RC frames, typically found in developing countries. Shake table tests were conducted on 1:3 reduced scaled two-story RC frames that included a code conforming SMRF model and another non-compliant model. The later was similar to the code conforming model, except, it was prepared in concrete having strength 33% lower than the design specified, which is commonly found in the region. The models were tested on shake table, through multiple excitations, using acceleration time history of 1994 Northridge earthquake, which was linearly scaled for multi-levels excitations in order to study the structures' damage mechanism and measure the structural response. A representative numerical model was prepared in finite element based program SeismoStruct, simulating the observed local damage mechanisms (bar-slip and joint shear hinging), for seismic analysis of RC frames having weaker beam-column joints. A suite of spectrum compatible acceleration records was obtained from PEER for incremental dynamic analysis of considered RC frames. The seismic performance of considered RC frames was quantified in terms of seismic response parameters (seismic response modification, overstrength and displacement amplification factors), for critical comparison.

Keywords: SMRF; response modification factor; nonlinear modelling; over strength; displacement amplification factor

1. Introduction

Recent field surveys in developing countries (Badrashi *et al*. 2010) have shown a number of construction deficiencies including the use of substandard quality of materials and poor detailing practices. Among these, the use of low strength concrete less than the design specified is very common (Badrashi *et al*. 2010). Furthermore, recent experimental studies conducted on deficient RC frame built in low strength concrete have shown significant flexural cracking in beam-column members and severe joint panel damages under lateral loads well-below the design level demands (Ahmad *et al*. 2019a). Such joint damage can result in brittle shear hinging at local level and soft-storey mechanism at global level (Calvi *et al.* 2002, Pampanin *et al.* 2002, Sharma *et al.* 2012). Reinforced concrete structures if not built properly can result in catastrophic failure and subsequent human and economic losses, upon subjecting to earthquake induced strong ground motions (Ruiz-Pinilla *et al.* 2016, Erdil 2016, Ates *et al*. 2013, Rossetto and Peiris 2009, Arslan and Korkmaz 2007, Inel and Meral 2016). The above facts make it essential to assess the performance of the existing building stock, taking into account the structural- and regional-specific deficiencies, for seismic safety evaluation under various hazard levels, which will aware the public about the potential risk of their buildings.

The present paper presents experimental and numerical investigation carried out on two reinforced concrete special moment resisting frames (SMRFs) that included a code-conforming model designed to the seismic building code and a non-compliant model SMRF with a construction defect of having low strength concrete of 2000 psi (14 MPa), typically found in developing countries. Shake table tests were performed on 1:3 reduced scale representative models, which were excited using natural acceleration time history of 1994 Northridge earthquake with multiple excitations (5-to-100% of the peak ground acceleration). The damage mechanism of each model was observed and reported. Acceleration and displacement response of the specimen were recorded and analyzed to obtain the lateral force-deformation capacity curves for the considered structures, which were analyzed to calculate the structures' seismic response parameters i.e., stiffness, strength and ductility, and to analytically calculate seismic response modification factor R using the classical formula based on Newmark and Hall (1982). A finite element based nonlinear model of the tested frames was developed in the finite element based software SeismoStruct 2016 (SeismoSoft 2016), taking into account the inelastic behavior of beam-column members, rebar-slip and joint shear hinging. The models were validated and calibrated with the experimentally observed roof displacement response and base shear demand. A suite of ten design spectrum compatible acceleration records was retrieved from the PEER NGA strong ground motions database and employed for incremental dynamic analysis of the models to derive

*Corresponding author, Ph.D.
E-mail: naveed.ahmad@uetpeshawar.edu.pk
[a]Lecturer
[b]Postgraduate Advisor

ISSN: 2092-7614 (Print), 2092-7622 (Online)

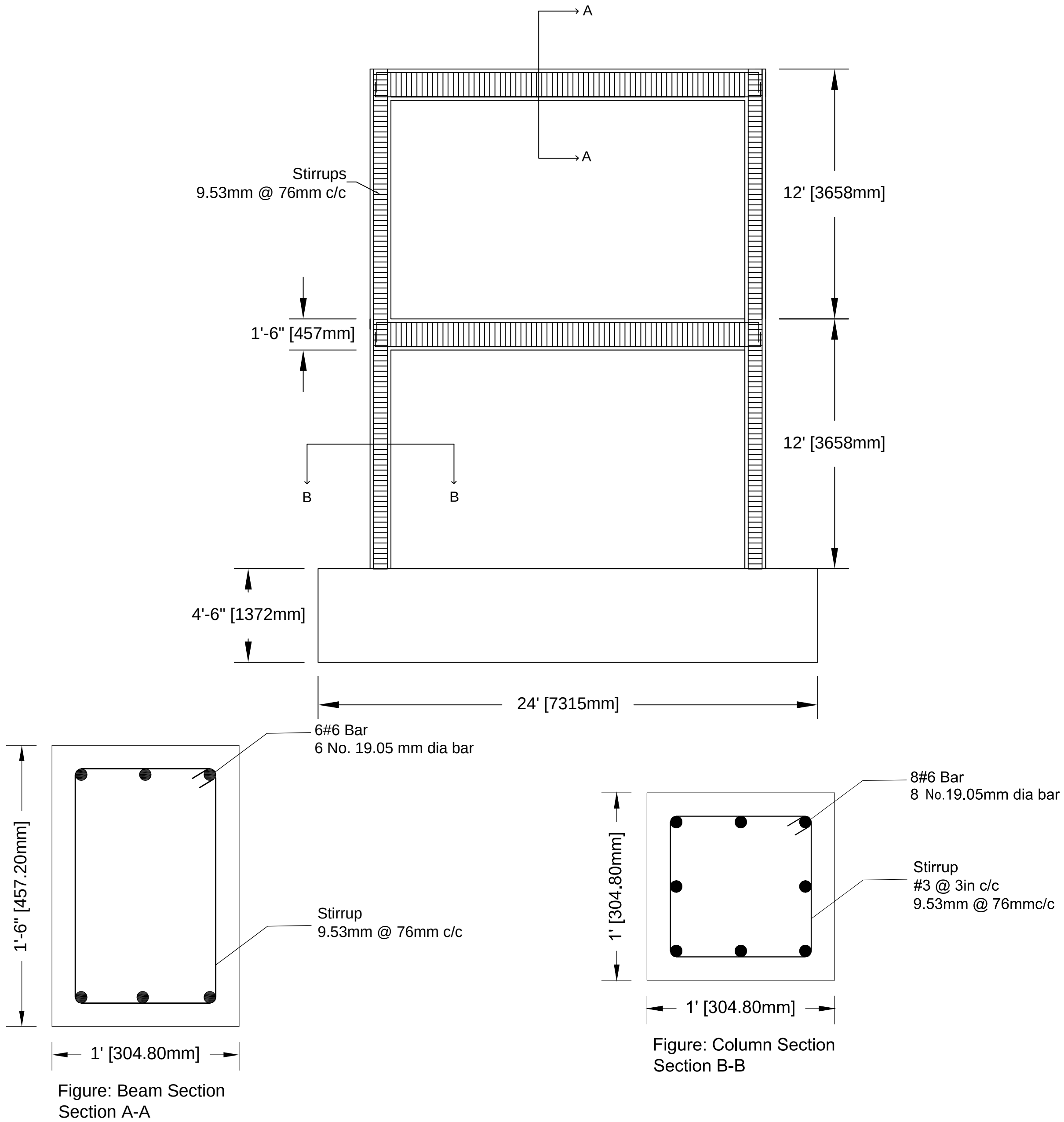

Fig. 1 Layout of the considered RC frame model

the structural capacity curves and response curves, which were used for the computation of overstrength based and ductility based factors to calculate the structures' response modification factor R.

The present research program comprised of two phases: the experimental part of the research that included the design and construction of model and shake table testing, and the second phase included the development and validation of FE based modeling and extension for the IDA and calculation of R factor. The following sections describe the experimental study carried out as part of the research.

2. Experimental program

2.1 Description of prototype structures

The considered frame was designed using the lateral static force-based seismic design procedure specified in the BCP-SP (2007), which is compatible to the UBC-97. The structure design was carried out for the high seismic hazard (Zone 4, 0.40g design PGA on soil type B) and detailed as per the ACI-318 (2005) recommendations for SMRF. The structure loading included self-weight for structural beam-column members and floor and roof slab, superimposed dead load for floor finishes and loads for partitions/contents. Concrete with compressive strength of 3000 psi (21 MPa) and reinforcing steel bars with yield strength of 60,000 psi (414 MPa) were considered. The structure design was carried out in the finite element based software ETABS CSI (ETABS 2009), considering all the load combinations for dead, live and earthquake loads as per the BCP-SP (2007). Fig. 1 shows the geometric and

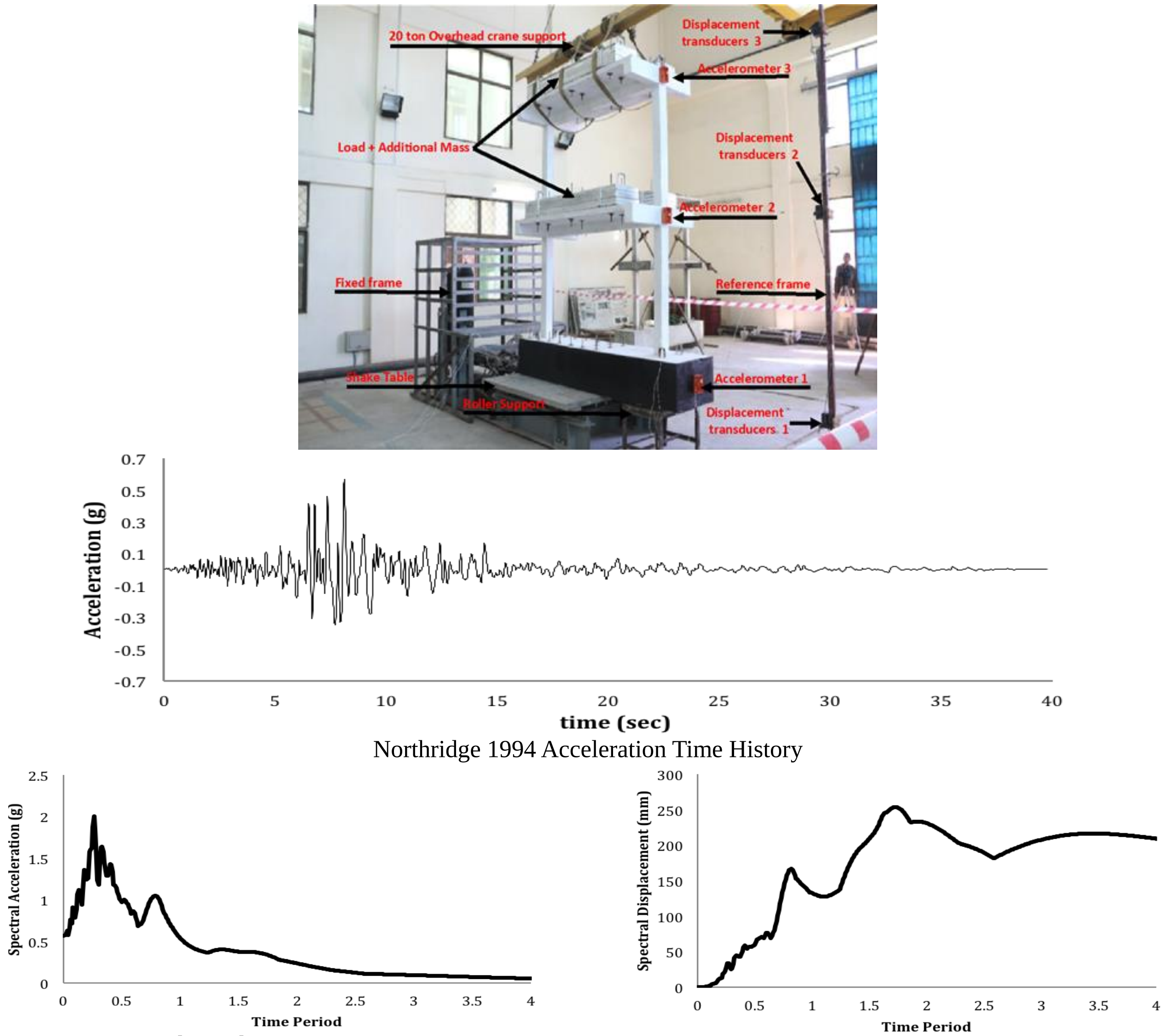

Northridge 1994 Acceleration Time History

5% Damped Acceleration Response Spectra

5% Damped Displacement Response Spectra

Fig. 2 Final test model and instrumentation plan and in Input excitation for shake table test models

reinforcement details of the designed structure.

As mentioned earlier that the execution of specified designs in the field is a major challenge in many developing countries till now, due which numerous defects can be found in the existing buildings (Badrashi *et al.* 2010). The present study considered two structure models (as shown in Fig. 1) to investigate the effects of low strength concrete. Model-1 is conforming to the code design specification with a concrete strength of 3000 psi (21 MPa), Model-2 is conforming to the code specified reinforcement detailing but having lower concrete strength of 2000 psi (14 MPa).

2.2 Preparation of 1:3 reduced scale test models

A simple model idealization was considered in which the materials' stress-strain properties essentially remained the same for both the prototype and model. All the linear dimensions of beams, columns and slabs and diameter of the steel re-bars were reduced by a scale factor S_L 3. Concrete for the 1:3 reduced scale model was prepared with a mix proportion of cement, sand and 3/8 inch (9 mm) down coarse aggregate to respect also the aggregate scaling requirements for models' concrete. The ACI concrete mix design procedure was followed for the preparation of concrete with compressive strength of 3000 psi (21 MPa) for the code conforming model and 2000 psi (14 Mpa) for low strength concrete model. A mix proportion of 1:1.80:1.60 (cement: sand: aggregate) with a water-to-cement ratio of 0.48 is used to achieve 3000 psi (21 MPa) and mix proportion of 1:3.50:2.87 (cement: sand: aggregate) with a water-to-cement ratio of 0.80 is used to achieve 2000 psi (14 MPa). It is worth to mention that the model and prototype uses essentially the same materials type (concrete and steel re-bars), which have similar stress-strain behavior and material density (unit weight). Due to this, the reduced scale models were subjected to gravity and seismic mass less than the required as per the similitude requirements for prototype-to-model conversion as shown in Eqs. (1) and (2)

$$M_r = \frac{M_m}{M_p} = L_r^2 \quad (1)$$

$$L_r^2 = \frac{1}{S_L^2} \quad (2)$$

where M_r is the ratio of model mass M_M to prototype mass M_P, L_r is the reciprocal of linear scale factor S_L. In order to satisfy the above requirements for complete model mass simulation, the additional required mass were applied to each floor of the model, calculated following the mass simulation model of Quintana-Gallo *et al.* (2010), as given in Eq. (3)

$$M_{M1} = \frac{M_p}{S_L^2} - M_{M0} \quad (3)$$

where M_{M1} is the additional floor mass for model, M_{M0} is the floor mass of model. The total mass on each floor is, thus, the sum of additional mass M_{M1} and M_{M0}, the result into an additional mass of 1200 kg for each floor.

2.3 Instrumentation and loading protocols

The test model was instrumented with six accelerometers with maximum capacity of ±10 g and three displacement transducers with maximum capacity of 24 inch (610 mm). Two uni-axial accelerometers (front and back) were installed on each floor and base pad to record the in-plane acceleration of the model. For in-plane lateral displacement measurements, a fixed steel reference frame was erected in-lined with the model. The displacement transducers were mounted on the reference frame; the transducers' strings were stretched by half-length of 12 inch (305 mm) and attached to each floor and base pad, keeping the table positioned at mid-way of ±125 mm displacement. The instrumentation scheme is shown in Fig. 2.

The experimental tests were conducted on the models in a fully dynamic environment by means of uni-directional seismic simulator (shake table). A natural acceleration time history record of 1994 Northridge earthquake (horizontal component, 090 CDMG Station 24278-PEER strong motion database) was selected as an input excitation after careful analysis of number of accelerograms. This record has maximum acceleration of 0.57 g, maximum velocity of 518 mm/sec and maximum displacement of 90 mm, and can laterally excite the structure symmetrically in both positive/negative directions.

After the shake table self-check run for system adjustment, the selected acceleration time history was applied to the test model with multiple excitations - 5%, 10%, 20%, 30%, 40%, 50%, 60%, 70%, 80%, 90%, 100% and 130% of the maximum acceleration of record, to push the structure from elastic to inelastic and incipient collapse state. Each of the specimen was tested progressively and their damage behavior was observed after every run, the tests were concluded when the test model were found in the incipient collapse state.

2.4 Damage mechanism of tested specimens

Model 1: This model was first subjected to a self-check excitation that pushed the structure laterally to about 1.88% roof drift, which was under the seismic simulator's automatic run before subjecting the structure to multiple excitations; the shaking intensity of this excitation was found to have maximum acceleration of 0.60 g. During this run the model was observed with significant flexure cracks in the beam on the ground story due to flexure yielding of reinforcing steel and formation of plastic mechanism at the beam-ends. Slight vertical cracks were observed in the beam on ground story at the beam-column interface, which is due to the beam's longitudinal steel bars slip. Flexure cracks were also observed in the columns' base on the ground story. Slight flexure cracks were also observed at the beam-ends on the first story.

Upon subjecting the model to increased intensity 100% of the input excitation (experiencing 0.62 g as maximum input acceleration), the model damages remained fairly the same. The previous damages in the model significantly aggravated upon subjecting to 130% of the input excitation (experiencing 1.06 g as maximum input acceleration). During this run, the model was observed with concrete crushing and core spalling at the base and top ends of the columns on the ground story due to excessive compressive strain demand on the cover concrete. Minor spalling was also observed at the base of columns on the first story. Additionally, the model was observed with severe diagonally cracks in the joint panel region on the ground story and slight diagonal cracks in the joint region on the first story, which is due to transferring moments from beam-ends to columns' ends. This damage points to the existence of materials' over-strength in beams that resulted in plastic section moment capacity higher than the yield moment capacity, consequently, increasing demands on the joint region. The model was found in the incipient collapse state. Fig. 3 shows the observed damages of the model.

Model 2: This model did not receive any visible crack upon subjecting to self-check excitation automatic run that pushed the structure laterally to about 0.50% roof drift, which is due to the fact that the intensity of the self-check excitation was significantly lower (experiencing 0.30 g as maximum input acceleration). After the self-check, the structure was subjected to further multiple excitations progressively. Initially, under the first significant regular run the model experienced lateral roof drift of 2.09%. The model in this run was observed with slight flexure cracks at the bottom of columns on the ground story and significant flexure cracks at the bottom of columns on the first story. Slight diagonal cracks were also observed in the joint region on ground story. Slight vertical cracks were observed also at the beam-column interface at the beam-ends on both ground and first story. On further higher intensity excitations the damages in the model aggravated. Under the 70% run the model experienced lateral drift of 3.33%. During this run the existing cracks in the columns' base at the ground and first story and cracks in the joint regions widened significantly. Minor spalling was observed at the base of columns on the first story. Additionally, flexure cracks were appeared also at the beam-ends on both the ground and first story. Further increasing excitations, the

Fig. 3 Damage evolution of code conforming model and low strength concrete model

model under 80% run the model experienced a roof drift of about 5.08%. In this run the model was severely damaged, experiencing concrete crushing and cover spalling at the top and base of columns on the ground and first story. Joint regions on both the ground and first story were observed with extreme damages, in the form of diagonal bat-like cracks. However, damages in the first story joints were relatively severe, which were observed with bat-like cover concrete wedge detachment from one side of the top right joint. The base shear strength of the model was dropped by about 4%, the model in this state was found in the near collapse state. Upon further subjecting the model to 90% run, the model experienced roof drift of 7.01%. The existing damages in the model further aggravated, however, the damages were relatively larger on the first story. Bat-like concrete cover wedge were detached from the joint regions of first story; the longitudinal steel bars of columns were visible through the joint panels. The base shear strength of the model was dropped by about 21%, the model after this run was in the incipient collapse state. Fig. 3 shows the observed damages of the model.

Model-2 has been observed to deform laterally to larger roof drift under similar input excitations. Unlike Model-1, Model-2 experienced damages in joints quite earlier and to extreme extend under significantly lower excitations. This is due to the fact of using low strength concrete in SMRFs. This reduces the steel-to-concrete bond strength and allows steel bars slip through concrete, consequently resulting in larger displacement of the model. Such bar-slip phenomenon has been observed also under quasi-static cyclic tests on special moment resisting beams[32]. Furthermore, the joint panels damaged under less shear demands (in transferring beam moments to columns) due to the lower principal tensile strength of the joint panel. Since, the joint principal strength capacity primarily depends on the strength of core concrete that is related to the compressive strength of concrete.

Comparison of Model 1 and Model 2: Fig. 4 shows the observed response of Model-1 and Model-2 for multiple excitation levels in terms of seismic excitation levels and seismic displacement demand. Model-1 has performed as per the code presumptions; forming plastic hinges in the beam-ends and cracking in column at the base and very few slight cracks in joint panels under the design level excitation, and deforming to lateral displacement within the code allowable drift.

In comparison to Model-1, Model-2 has been observed to deform laterally to larger roof drift under similar input excitations. Model-2 experienced damages in joints quite earlier and to extreme extend under significantly lower excitations. This is due to the fact of using low strength concrete in SMRFs, that reduces the steel-to-concrete bond

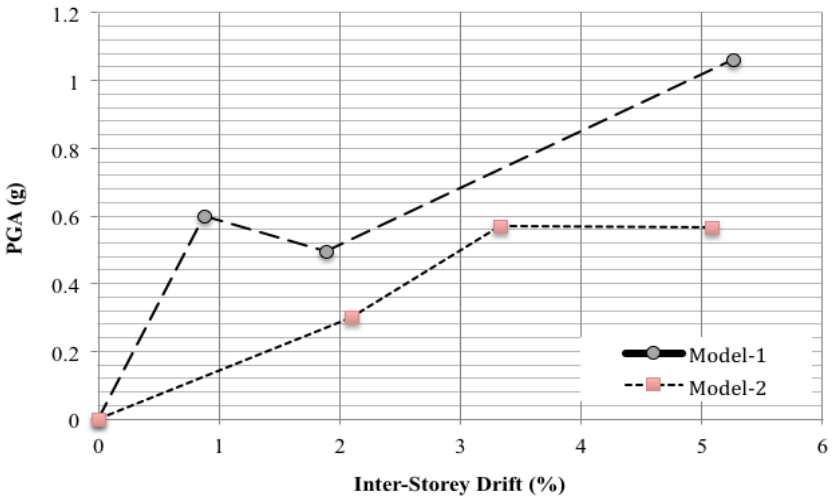

Fig. 4 Seismic response curves (input PGA versus roof displacement) for prototype structure

Table 1 Observed damages and structural response under design level earthquake excitation

Tested Model	Run	Roof Displacement inch (mm)	Roof Drift (%)	Base Shear kips (kN)	Observed Damages
SMRF Code Design Model-1	100% (0.49 g)	5.26 (133.56)	1.88	42.47 (188.90)	- Significant flexure cracks were observed at the beam-ends on the ground storey. - Slight vertical cracks were also observed at the beam-ends at beam-column interface. - Slight flexure cracks were observed also at the beam-ends on the first floor. - Flexure cracks were observed at the base of ground storey columns. - Hairline cracks were also observed at the column top on the ground storey columns. - Slight flexure cracks were also observed at the base of columns on the first floor.
SMRF Low Strength Concrete Model-2	90% (0.6 g)	19.56 (496.95)	7.01	33.68 (149.83)	- The damages in beam and column members aggravated significantly, with more damages on first storey. - Bat-like concrete cover wedge were detached from the joint regions of first storey; - Longitudinal steel bars of columns were visible through the joint panels. The model was in the incipient collapse state.

strength and allows steel bars slip through concrete, consequently resulting in larger displacement of the model. Such bar-slip phenomenon has been observed also under quasi-static cyclic tests on full-scale special moment resisting beams and shake table tests on RC frame (Rashid and Ahmad 2017, Ahmad *et al.* 2018). The joint panels damaged under less shear demands due to the lower principal tensile strength of the joint panel concrete, which is related to the compressive strength of concrete (Pampanin *et al.* 2002, Priestley 1997).

3. Numerical modeling

The earlier section described the experimental response of the test model under a single acceleration time history. In order to take into account the record-to-record variability in the seismic response of structures, and calculation of response parameters, numerical analysis of the test model became essential. The nonlinear numerical modeling technique, as proposed earlier by Ahmad *et al*. (2018) for inelastic seismic analysis of RC frames and incorporated in finite element based software SeismoStruct 2016, was extended for nonlinear time history analysis of both code-compliant and code non-compliant tested RC frames. The modeling technique is capable of simulating both the global structural displacement response and local mechanisms (flexure hinging of beams and columns and shear hinging of joint panels). Fig. 4 shows the representative prototype of the tested RC frame while Fig. 5 shows the idealized equivalent frame prepared in SeismoStruct 2016 for nonlinear analysis.

3.1 Description of proposed numerical RC frame nonlinear model

3.1.1 Beam and column elements modelling

The proposed modeling technique makes use of inelastic

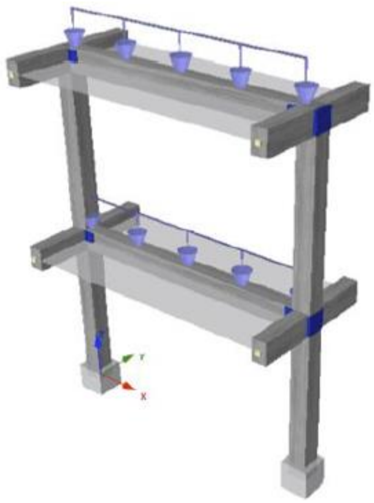

Fig. 4 Representative of finite element based prototype develop in SeismoStruct

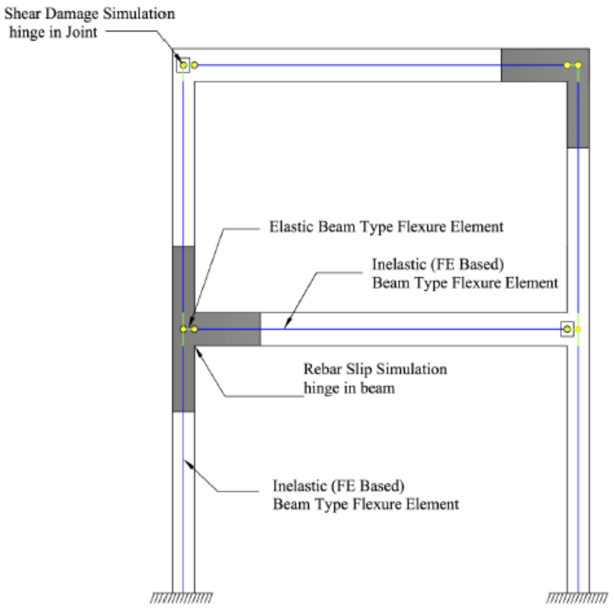

Fig. 5 Idealization of nonlinear inelastic modelling of considered RC Frame structure

flexural beam type element, which uses FE forced-based formulations (Neuenhofer and Filippou 1997, Spacone *et al.* 1996),). The force-based inelastic flexural beam type elements are capable of capturing the material inelasticity and geometrical nonlinearly of the members under cyclic loading and deformation. Earthquake engineering researchers worldwide usually employ distributed plasticity element for nonlinear modeling and seismic analysis of structures for static and time history analysis, due to the widespread calibration and validation of the technique, and economy in the computational cost (Filippou and Fenves 2004, Fragiadakis and Papadrakakis 2008).

In the fiber-based section of SeismoStruct, the RC member section is divided in to confined concrete fibers, unconfined concrete fibers and reinforcement steel fibers as shown in Fig. 6. All these discrete fibers are assigned with uniaxial material stress-strain relationships.

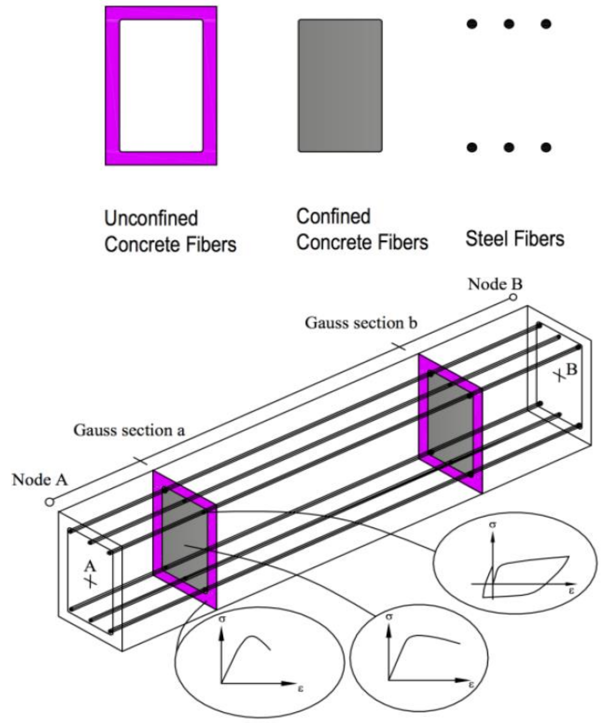

Fig. 6 Idealizing beams and columns as inelastic FE forced based flexural type element, SeismoStruct (2016)

By integrating the nonlinear stress-strain response of each fiber, the sectional stress-strain response is found. Such approach account for the spread of plasticity along the member length and across the section depth. Typically the section is subdivided in to 100 to 400 fibers depending upon the accuracy required. The advantages of such models are; no prior moment-curvature analysis is required, hysteretic response of the element is not needed as it is implicitly simulated through material constitutive models, interaction between flexural strength in orthogonal directions, clear representation of biaxial bending and direct modeling of axial load-bending interaction.

In the current version of SeismoStruct (2016) eleven different element types are employed, which can be used to represent and model accurate structural and non-structural components (beams, column, joint panel, wall, infill panels, dissipating devices, etc.) response and can also be used for special boundary condition problems. In the 2016 version of the SeismoStruct 2016, eleven material types are available for the users to model different types of material (like concrete, steel, shape-memory alloys and elastic material).

In the current study, the Mander *et al*. nonlinear concrete material model was used for modelling concrete (Fig. 7(a)). The program automatically accounts for the effects of confinement on the enhancement of section's strength and ductility. The cyclic behavior of longitudinal steel re-bars was simulated using the Menegotto-Pinto steel model (Fig. 7(b)).

3.1.2 Joint modelling

Many numerical and analytical models have been recently proposed for simulating the nonlinear hysteric behavior of RC beam-column joint (Celik and Ellingwood

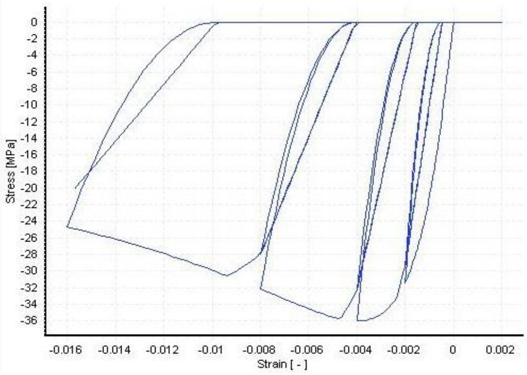

(a)

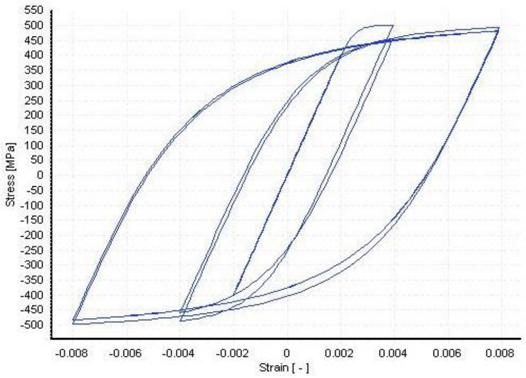

(b)

Fig. 7 (a) Mander et al Concrete and (b) Menegotto-Pinto Steel stress-strain models, SeismoStruct (2016)

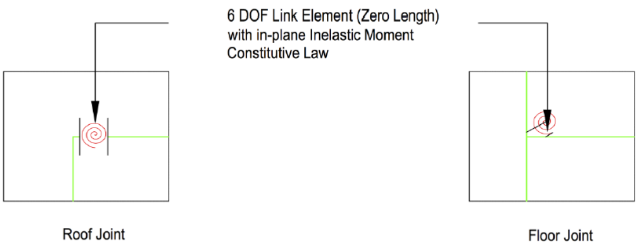

Fig. 8 Idealizing and modeling joint nonlinear hinge

2008, Alath and Kunnath 1995, Biddah and Ghobarah 1999, Youssef and Ghobarah 2001, Lowes and Altoontash 2003, Fan *et al.* 2018, Lima *et al.* 2017, Adom-Asamoah and Banahene 2016). In most of these modeling techniques, the main input is the moment transferred through rotational spring that simulates joint deformation (Celik and Ellingwood 2008). In this study a simplified numerical modeling technique is proposed for simulating joint panel damageability. This included idealizing joint panel with stiff elastic flexure beam type elements provisioned with a zero-length link element at the joint center that connects the joint horizontal element with the vertical elements through a rotational spring as shown in Fig. 8. The joint panel link is provisioned with the moment-rotation spring assigned with the multilinear constitutive law (Sivaselvan and Reinhorn 2001) to simulate the joint shear hinging.

For simulating the joint deformation and transferring the joint shear stresses into equivalent moment rotation capacity of the rotation spring, the scissor model proposed

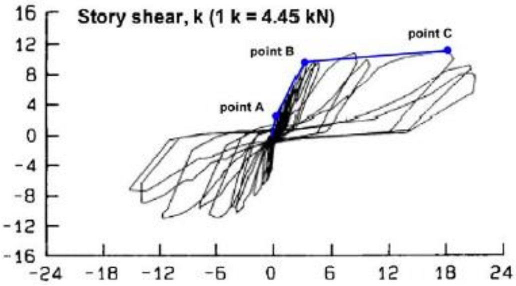

Fig. 9 Key points showing distinct stiffness change global and local response (Kim and LaFave 2012)

by Alath and Kunnath (1996) is employed with degrading hysteric behavior. Based on shear model proposed by Alath and Kunnath, the spring rotational moment capacity can be expressed in terms of the joint shear stress and sectional dimensions

$$M_j = \tau_j A_{jh} \frac{1}{\left(\frac{1-\frac{b_j}{L_b}}{jd} - \frac{1}{L_c} \right)} \tag{4}$$

where M_j is the rotational spring moment capacity; τ_{jh} is the joint shear strength, corresponding to diagonal tensile strength of joint; A_{jh} is the joint shear area $A_{jh}=b_j \times h_j$, b_j represents the joint panel width and h_j represents the joint panel depth; L_b is the total length of beam on left and right side of joint, between the contra-flexure points; L_c is the total length of column above and below the joint, between the contra-flexure points; j_d is the internal moment arm.

3.1.3 Joint shear strength model

The rotational spring moment capacity M_j, requires joint panel shear strength capacity τ_j. Many analytical and numerical models have been reported in literature for predicting the joint panel nonlinear shear-deformation behavior. The joint panels shear strength and deformation capacities, for both code compliant Model-1 and code non-compliant Model-2, have been modeled using the unified shear behavior model of Kim and LaFave (2012), which has been developed and tested against extensive experimental tests on RC beam-column joints under cyclic loadings, and considers the joint shear failure with and without beam longitudinal reinforcement yielding cases.

Based on the experimental data, key points with distinct stiffness changes have been identified, including cracking point, yield point and peak response point, as shown in Fig. 9. By connecting these distinct points, the joint panel shear stress-shear strain behavior envelope curves for the overall cyclic and local cyclic response can be obtained. In Fig. 9, A is the point where initial stiffness changes considerably as compared to the tangent stiffness. Similarly at point B, the tangent stiffness distinctively changes from point A. Point C is the peak behavior for either the global or local response. Kim and LaFave (2012) reported that these stiffness changes in the global behaviors typically correspond to similar stiffness changes in the local behaviors, which

Table 2 Simplified joint shear stress and shear strain model, Kim *et al*. (2012)

Distinct Point	Equation
Point A	V_j at point A = 0.442 x Equation 5 γ_i at point A = 0.0197 x Equation 6
Point B	V_j at point B = 0.890 x Equation 5 γ_i at point B = 0.362 x Equation 6
Point C	$V_j\ at\ peak\ point\ (MPa) =\ \alpha_t\ x\ \beta_t\ x\ \eta_t\ x\ \lambda t\ x\ JI^{0.15}\ x\ BI^{0.30} x\ fc'^{0.75}$ (5) $\gamma_j\ at\ peak\ point\ \mathrm{C}\ (Rad) =\ \alpha_{\gamma t}\ x\ \beta_{\gamma t}\ x\ \eta_{\gamma t}\ x\ \lambda_{\gamma t}\ x\ BI\ x\ (JI)^{0.10}\ x\ \left(\frac{V_j}{fc'}\right)^{-0.75}$ (6)
Point D	V_j at point D = 0.90 x Equation 5 γ_i at point D = 2.02 x Equation 6

depicts that joint panel local damages can cause global overall stiffness changes.

Using the probabilistic Bayesian parameter estimation method, Kim et.al developed the simplified RC joint shear stress and shear strain model for the peak response i.e., point C as:

For peak shear stress i.e. point C

$$Vj \text{ at peak response} =$$

$$\alpha_i \times \beta_i \times \eta_t \times \lambda_t \times JT^{0.15} \times BI^{0.30} \times f_c^{0.75}\ (MPa) \qquad (5)$$

whereas in equation

α_t = a parameter for describing in-plane geometry:
1.0 for interior connections,
0.7 for exterior connections and
0.4 for knee connections;

β_t = Parameter for describing out-of plane geometry:
1.0 for subassemblies with zero or one transverse beam and
1.18 for subassemblies with two transverse beams

$\eta_t = (1-\frac{e}{bc})$^0.67 , for joint eccentricity
1.0 for no eccentricity

λ_t = 1.31, Parameter suggested by Kim *et al* for the simple unified equation.

JI = Joint transverse reinforcement index, JI = $(\frac{\rho_j\ x\ fyj}{fc'})$

ρ_j = Volumetric joint transverse reinforcement ratio in the direction of loading

f_{yj} = joint transverse reinforcement yield stress

BI = Beam reinforcement index, BI = $(\frac{\rho_b\ x\ fyb}{fc'})$

ρ_b is the beam reinforcement ratio and

f_{yb} is the yield stress of beam reinforcement

f_c' = Concrete compressive strength

Similarly the simplified RC shear joint deformation models at peak response i.e., at point C suggested by Kim et al. is

$$\gamma j \text{ at peak response} =$$

$$\alpha_{\gamma t} \times \beta_{\gamma t} \times \eta_{\gamma t} \times \lambda_{\gamma t} \times BI \times JI^{0.10} \times \left(\frac{\tau_j}{f_c^i}\right)^{-1.75} (rad) \qquad (6)$$

whereas in equation

$\alpha_{\gamma t}$ = Parameter for describing in-plane geometry

$\beta_{\gamma t}$ = Parameter for describing out-of-plane geometry
1.0 for subassemblies with zero or one transverse beam
1.4 for subassemblies with two transverse beams

$\eta_t = (1-\frac{e}{bc})$^-0.6 , describes joint eccentricity

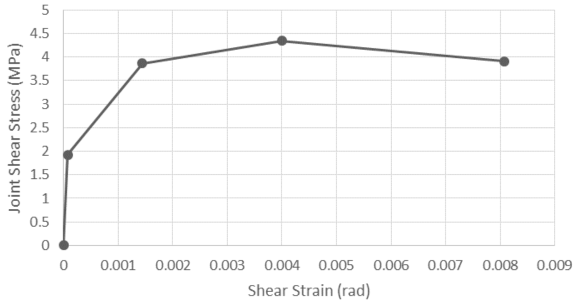

(a)

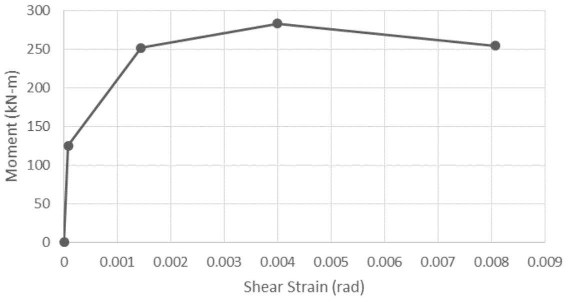

(b)

Fig. 10 Model-1 Joint panel shear stress-shear strain relationship (b) Model-1 Joint panel equivalent moment-rotation relationship

1.0 for no eccentricity

$\lambda_{\gamma t}$ = 0.0055, a parameter suggested by Kim *et al*. for the simple unified equation.

Table 2 reports the RC beam-column connection shear stress-shear strain relationship developed by Kim and LaFave (2012), for four key points; including a post peak descending behavior i.e., point D which is suggested as 90%, as shown in Table 2. Although the joint shear strength and deformation behavior are derived for the experimental cases, where beam-column connections are provided with confine transverse reinforcement, these shear stress and shear strain behavior model equations can still be used for joint panels without transverse reinforcement cases. Kim *et al*. suggest a virtual value of JI equal to 0.0139 for RC beam-column joint with no transverse reinforcement cases. Fig. 10(a) shows shear stress and shear strain relation and Fig. 10(b) shows equivalent moment and rotation (shear-stain) relation developed for the code compliant Model-1 using the Alath and Kunnath (1996) scissor hinge moment capacity model and Kim and LaFave (2012) joint shear behavior model.

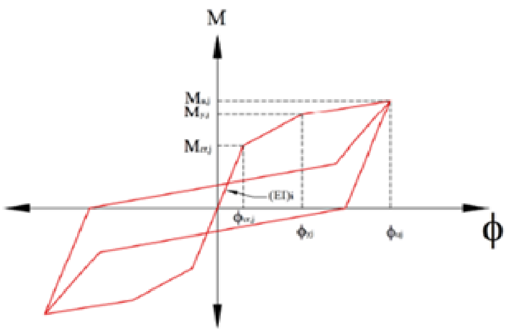

Fig. 11 Joint shear hinge constitutive relation (Sivaselvan and Reinhorn 2001)

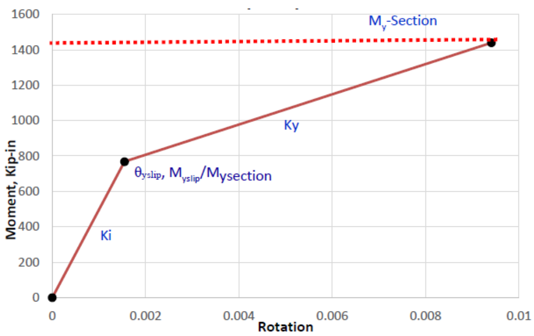

Fig. 12 Bi-linear backbone idealization for bar slip simulation

3.1.4 Joint panel hysteretic constitutive model

After defining the backbone curve of joint panel, cyclic hysteretic rules must be employed to implement constitutive relationships. In this study the moment rotation spring is assigned with multi-linear constitutive law (Sivaselvan and Reinhorn 2001), currently available in SeismoStruct, to capture the cyclic hysteric behavior of joint panel behavior. Experimental studies on beam-column joints with no transverse reinforcement reveals degrading and highly pinched shear stress-shear strain behavior. Fig. 11 show the hysteric constitutive model of joint shear hinge employed for the code compliant and code non-compliant specimens.

3.1.5 Bar-slip modeling

Beam longitudinal reinforcement slip and yielding causes additional deformations in the form of fixed end rotations at the beam-column interface (Caprili *et al*. 2018). Paulay and Priestley (1992) have noted that such deformations, due to the opening of cracks at the beam-column interface, contribute to the total member deformation (i.e., chord rotation) by about 50%. In the present study, a moment rotation spring with bi-linear moment rotation envelope is assigned at the beam-ends, in order to capture bar-slip and fixed-end rotation mechanism of the beam member. Using a post-hardening bi-linear constitutive law (Fig. 12), the in-plane rotational spring is modeled through beam-end links, which is in series with the beam fiber element. Experimental quasi-static cyclic tests conducted on full-scale SMRF RC beams (Rashid and Ahmad 2017, Ahmad *et al*. 2018) were analyzed for the computation of rotational spring constitutive parameters (Fig. 12).

Table 3 Experimental to numerical comparisons Model-1

100% Run	Max Roof Displacement (mm)	Max Base Shear, VB (kN)
Experimental	145.19	181.4
Analysis	144.35	166.78
% Error	**0.58 %**	**8.05 %**

Table 4 Experimental to numerical comparison Model-2

10% Run	Max Roof Displacement (mm)	Max Base Shear, VB (kN)
Experimental	147.9	163.6
Analysis	148.8	148.6
% Error	**-0.57%**	**9.17%**

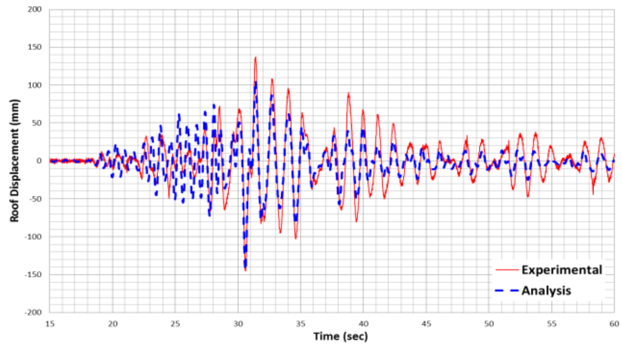

Fig. 13 Top storey displacement time history Model-1

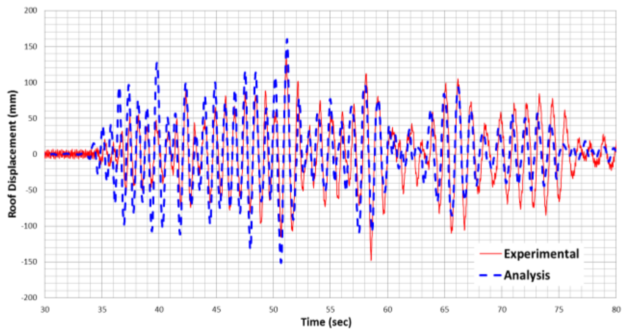

Fig. 14 Top storey displacement time history Model-2

3.2 Validation of the proposed numerical modelling

Following the aforementioned modeling approach, nonlinear numerical models were developed for the tested models in SeismoStruct v. 2016. The numerical models were first validated against the experimental tests in predicting the roof displacement response and peak shear and displacement demand.

The model (beam members) was loaded with the imposed super dead load of floor finish and 25% of live load, in order to simulate the seismic weights. The numerical FE model was subjected to the input acceleration, recorded at the base of the model during shake table tests. The numerical modeling technique was evaluated in predicting the peak roof displacement and peak base shear demands, and local damage mechanisms (beam bar-slip, beam/column flexure hinging and joint cracking & damage). Table 3 and Table 4 report the comparison of numerical prediction to experimental observations, which shows reasonable performance of the modeling technique. Fig. 13 and Fig. 14 compare the numerically obtained roof displacement to the experimentally observed response. The comparison of numerical predictions to experimental observations has revealed promising behavior of the modeling technique in predicting the roof displacement response and peak demands in terms of roof displacement and base shear force. The technique was also reasonable in simulating the local damage mechanisms like beam/column hinging, bar-slip and joint panel damage.

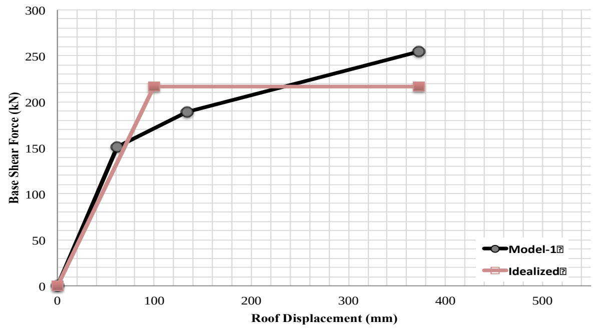

(a) Model-1, Code Conforming

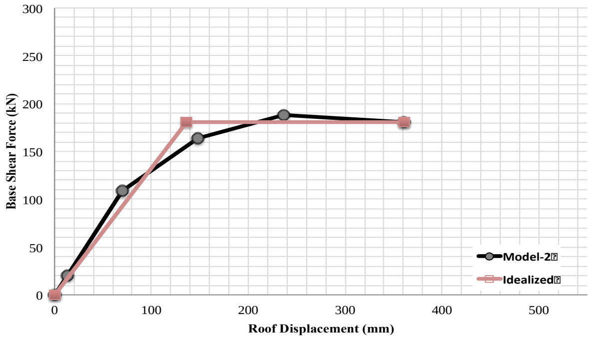

(b) Model-1, Code Conforming

Fig. 15 Force deformation behaviour of RC frames

4. Response modification factor (R- Factor)

4.1 R-Factor based on experimental investigation

The present study included both the experimental and numerical approaches to calculate R factor. The experimental approach involved the derivation of lateral force-deformation capacity curve of models, and using the analytical formulae of Newmark and Hall (1982) to quantify R. Similar approach has been recommended and used in many earlier studies (Ahmad *et al.* 2019a, Akbar *et al.* 2018, Elnashai and Di-Sarno 2008, Rizwan *et al.* 2018). By definition, R factor of a structure is the reduction required to reduce the elastic base shear force the structure will experience, if responding elastically

$$R = \frac{V_e}{V_s} = \frac{V_e}{V_y} \times \frac{V_y}{V_s} = R_\mu \times R_s \tag{7}$$

where V_e represents the elastic force the structure will experience, if respond elastically under earthquake demand; V_y represents the idealized yield strength of the structure; V_s represents the design base shear force; R_μ represents the 'ductility factor', structure ductility dependent factor, R_S represents the 'overstrength factor', structure overstrength dependent factor. The overstrength factor R_S is calculated directly from the lateral force-deformation capacity curve of the structure (i.e., dividing the idealized yield strength over the structure design base shear). The ductility factor R_μ is related to the structural ductility Newmark and Hall (1982), knowing the yield period of the structure, as given in Eq. (8)

$$\left.\begin{array}{c} \text{For } T < 0.20\,\text{sec} \\ R = 1.0 \\ \text{For } 0.20\text{sec} < T < 0.50\,\text{sec} \\ R = \sqrt{2\mu - 1} \\ \text{For } 0.5\text{sec} < T < 0.20 \\ R = \mu \end{array}\right\} \tag{8}$$

where T is the pre-yield vibration period of idealized single degree of freedom system. The weight of the considered prototype frame is 28 ton, and considering the yield stiffness obtained from the experimental idealized capacity curves, the structure vibration period was calculated using the classical formula of vibration period. The code specified ultimate drift limit of 2.50% is considered as the ultimate drift capacity that corresponds to displacement capacity of about 183 mm (7.20 inch). The frame ductility μ was obtained dividing the ultimate displacement capacity over the idealized yield displacement capacity of each structure model, which gives also an estimate of R_μ. The response modification factor R of prototype structures was calculated by multiply the ductility dependent R_μ factor with the overstrength factor R_S. For this purpose, the actual lateral-force deformation capacity curve derived herein experimentally was idealized as bi-linear elastic-plastic curve (Fig. 15) to identify the yield strength, yield displacement and ultimate displacement capacity. The idealization was carried out using the energy balance rule; to make the energy under the curve equivalent for both the actual and the idealized capacity curve. These idealized elastic-plastic curves were used to calculate the seismic response parameters of the structure and calculate *R*. The calculated *R* factor for code conforming frame is 7.5 for Model-1 and 4.5 for Model-2.

4.2 R-Factor based on numerical studies

The experimentally calculated R factor is based on the capacity curve derived through shake table tests on structure model using single accelerogram. Further, the calculation is based on the analytical model developed in earlier, which doesn't explicitly taking into account he energy dissipation of the considered structure. To take into account the variability in structure response due to differences in ground motions, and also to explicitly take into account the realistic energy dissipation capacity of the structure, a numerical approach was included to calculate *R*. This included the derivation of seismic capacity curve and structure response curve through incremental dynamic analysis of structure employing different natural accelerograms.

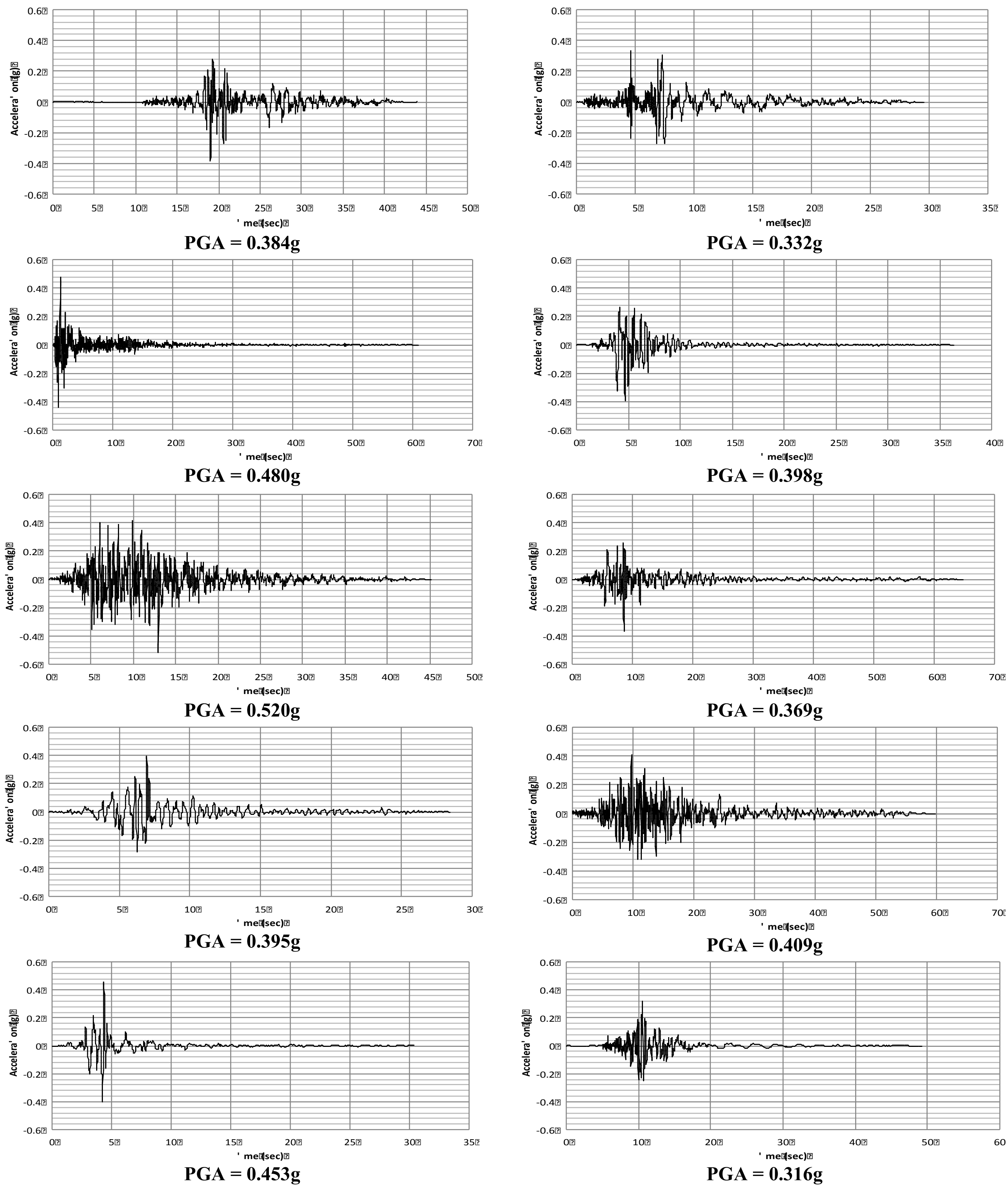

Fig. 16 Selected, scaled and matched accelerograms employed for incremental dynamic analysis

Various accelerograms were retrieved from the PEER NGA strong ground motions database, pre-specifying accelerograms search criterion that meets the regional tectonic characteristics of Pakistan. NGA-West 2 ground motions are considered with the following tectonic parameters; moment magnitude MW in the range of 6.0 to 8.0, faults specified with reverse/oblique mechanism, closest distance to fault rupture R_{jb} and R_{rup} are considered between 10 km to 30 km, considering a stiff soil with VS30 of 500 m/sec to 750 m/sec was specified. Furthermore, the accelerograms retrieved were carefully analyzed for selection, considering event-to-event and region-to-region

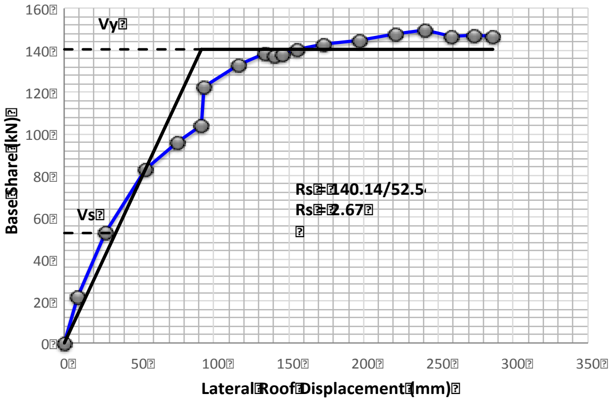

(a) Capacity Curve, IDA based derived

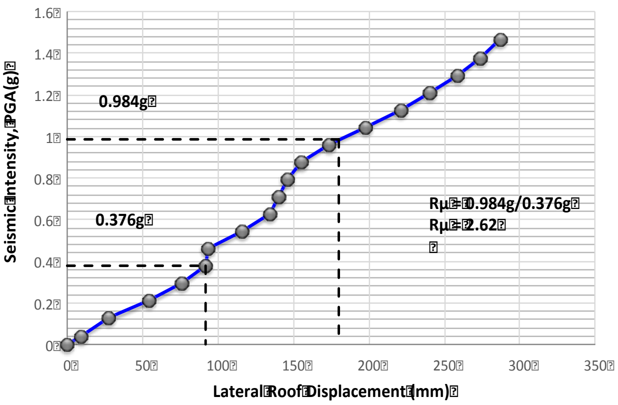

(b) Seismic Response Curve, IDA based derive

Fig. 16 IDA based derived seismic capacity curve and seismic response curve for Model-2

variability. The selected accelerograms were linearly scaled and matched, through wavelet-based approach employed in SeismoMatch, to design spectrum for seismic Zone 4 (design PGA=0.40 g).

The matched accelerograms were retrieved and linearly scaled up/down to multiple intensity levels. The numerical models were subjected to all the accelerograms and the incremental dynamic analysis procedure is adopted to derive the structure capacity curve, correlating the peak drift demand in each run with the corresponding base shear force, and the structure seismic response curve, correlating the peak drift demand in each run with seismic intensity. The capacity curve were bi-linearized and analyzed to calculate the structure overstrength R_S, which is the ratio of the yield strength to the design base shear, as described earlier. Analyzing the seismic capacity curve, the ductility factor R_μ is calculated as a ratio of the seismic intensity corresponding to the structure achieve the ultimate drift limit to the seismic intensity corresponding to the occurrence of yielding (global idealized yield, obtained from the dynamically derived capacity curve)

$$R\mu = \frac{PGA\ ultimate}{PGA\ yield} \tag{9}$$

The above approach for the calculation of ductility factor has been employed also in other recent studies (Ai *et al.* 2012, 2013, Ahmad *et al.* 2019b, Kappos 1991). Fig. 16 shows an example calculation of *R* factor for Northridge earthquake record for Model-2. Similarly, *R* factor for other acceleration records and models were calculated. An average value of 6.45 is obtained for Model-1 and 5.59 for Model-2, which can be approximated to 6.5 for Model-1 and 5.5 for Model-2, respectively.

Table 5 Final derived seismic response parameters

S. No.	Model	Response Modification Factor R	Over Strength Factor R_S	Displacement Amplification Factor C_d
1	Model 1	7.0	3.77	7.46
2	Model 2	5.0	3.10	4.00

5. Derived seismic response parameters:

As an outcome of the experimental and numerical research study conducted herein, seismic response parameters were derived (Table 5), averaging the experimental and numerical results. The derived parameters included seismic response modification factor (R), over strength (R_S) and displacement amplification factor (C_d).

The displacement amplification factor was calculated by performing analysis of representative elastic finite element numerical model under lateral loads, simulating floor forces. The floor forces were calculated based on the code specified distribution of base shear force. The analysis of elastic numerical model included both the seismic floor weights and lateral floor forces, which was analyzed through finite element based software SAP2000. The elastic roof displacement demand (Δ_e) obtained under the applied forces, and the displacement corresponding to code-specified allowed drift of 2.5%, representing ultimate displacement capacity (Δ_u), were used to calculate the displacement amplification factor

$$C_d = \frac{\Delta_u}{\Delta_e} \tag{10}$$

5. Conclusions

Experimental shake table tests were conducted on 1:3 reduced scale two-storey RC frames; one code conforming model and another deficient model that was prepared in low strength concrete. Observed damages of both complaint and non-compliant models have demonstrated that employing concrete of strength less than the design specified in construction alters the damage mechanism of RC frame from beam-sway mechanism to joint panel damage. This has resulted in the reduction of structural stiffness and strength and seismic response parameters; namely, response modification factor, overstrength and displacement amplification factor.

Inelastic modeling technique was presented for Finite Element based modeling of RC frames in SeismoStruct, capable to simulate the flexure hinging of beam-column members and shear hinging of joint panels. The presented modeling technique was tested and validated against the shake table tests, which have shown reasonable performance of the technique in simulating the lateral displacement time history response of both the code conforming model and deficient model, and in predicting the structure's peak displacement and peak base shear force demands.

Incremental dynamic analysis procedure was included for the derivation of structure's capacity curve and response curves. These were employed to compute the structure's overstrength and ductility factor, in order to calculate the structure response modification factor *R*. Furthermore, elastic numerical models were prepared in FE based software SAP2000, which were analyzed under the applied floor forces, representing the seismic forces for the design level base shear. The elastic roof displacement demand under the applied forces was calculated. Considering the code specified allowable drift capacity of 2.50%, the displacement amplification factor was calculated for each structure. On average, the code-conforming model exhibited *R* factor of 7.0, overstrength of 3.77 and displacement amplification factor of 7.46, while the deficient model exhibited *R* factor of 5.0, overstrength of 3.10 and displacement amplification factor of 4.0.

For the force-based seismic design of short period structures, commonly low-rise structures, the reduction in response modification factor will result in design base shear force 40% higher than the anticipated design base shear. This renders the structure vulnerable under earthquake lateral loads.

Acknowledgments

The authors thank the reviewers for the constructive remarks that improved the manuscript presentation. The research presented herein is part of the PhD Study of the first author in the Department of Civil Engineering of UET Peshawar under the supervision of Prof. Dr. Akhtar Naeem Khan (Professor, Department of Civil Engineering) and Dr. Naveed Ahmad (Postgraduate Advisor of Earthquake Engineering, Department of Civil Engineering).

References

ACI 318 (2005), Building Code Requirements for Structural Concrete and Commentary, American Concrete Institute, Farmington Hills, MI, USA.

Adom-Asamoah, M. and Banahene, J.O. (2016), "Nonlinear seismic analysis of a super 13-element reinforced concrete beam-column joint model", *Earthq. Struct.*, **11**(5), 905-924. https://doi.org/10.12989/eas.2016.11.5.905.

Ahmad, N., Akbar, J., Rizwan, M., Alam, B., Khan, A.N. and Lateef, A. (2019b), "Haunch retrofitting technique for seismic upgrading deficient RC frames", *Bull. Earthq. Eng.*, **17**(7), 3895-3932. DOI: https://doi.org/10.1007/s10518-019-00638-9.

Ahmad, N., Ali, Q. and Javed, M. (2019), "Force reduction factor R for shear dominated low-rise brick masonry structures", *J. Numer. Meth. Civil Eng.*, **2**(3), 14-29.

Ahmad, N., Shahzad, A., Ali, Q., Rizwan, M. and Khan, A.N. (2018), "Seismic fragility functions for code compliant & non-compliant RC SMRF structures in Pakistan", *Bull. Earthq. Eng.*, **16**(10), 4675-4703. https://doi.org/10.1007/s10518-018-0377-x.

Ahmad, N., Shahzad, A., Rizwan, M., Khan, A.N., Ali, S.M., Ashraf, M., Naseer, A., Ali, Q. and Alam, B. (2019a), "Seismic performance assessment of non-compliant SMRF reinforced concrete frame: shake table test study", *J. Earthq. Eng.*, **23**(3), 444-462. https://doi.org/10.1080/13632469.2017.1326426.

Akbar, J., Ahmad, N. and Alam, B. (2018), "Seismic performance of RC frames retrofitted with haunch technique", *Struct. Eng. Mech.*, **67**(1), 1-8. https://doi.org/10.12989/sem.2018.67.1.001.

Alath, S. and Kunnath, S.K. (1995), "Modeling inelastic shear deformations in RC beam-column joints", *Engineering Mechanics Proceedings of the 10th Conference*, University of Colorado at Boulder, Boulder, Colorado.

Ali, Q., Naeem, A., Ashraf, M., Ahmed, A., Alam, B., Ahmad, N., Fahim, M., Rahman, S. and Umar, M. (2013), "Seismic performance of stone masonry buildings used in the Himalayan Belt", *Earthq. Spectra*, **29**(4), 1159-1181. https://doi.org/10.1193/091711EQS228M.

Ali, Q., Schacher, T., Ashraf, M., Alam, B., Naeem, A., Ahmad, N. and Umar, M., (2012), "In-plane behavior of Dhajji-Dewari structural system (wooden braced frame with masonry infill)", *Earthq. Spectra*, **28**(3), 835-858. https://doi.org/10.1193/1.4000051.

Arslan, M.H. and Korkmaz, H.H. (2007), "What is to be learned from damage and failure of reinforced concrete structures during recent earthquakes in Turkey?", *Eng. Fail. Anal.*, **14**(1), 1-22. https://doi.org/10.1016/j.engfailanal.2006.01.003.

Ates, S., Kahya, V., Yurdakul, M. and Adanur, S. (2013), "Damages on reinforced concrete buildings due to consecutive earthquakes in Van", *Soil Dyn. Earthq. Eng.*, **53**, 109-118. https://doi.org/10.1016/j.soildyn.2013.06.006.

Badrashi, Y.I., Ali, Q. and Ashraf, M. (2010), "Reinforced concrete buildings in Pakistan-Housing Report", Housing Report No. 159, Earthquake Engineering Research Institute, CA, USA.

BCP-SP (2007), Building Code of Pakistan: Seismic Provisions-2007, Ministry of Housing and Works, Islamabad, Pakistan.

Biddah, A. and Ghobarah, A. (1999), "Modelling of shear deformation and bond slip in reinforced concrete joints", *Struct. Eng. Mech.*, **7**(4), 413-432. https://doi.org/10.12989/sem.1999.7.4.413.

Calvi, G.M., Magenes, G. and Pampanin, S. (2002), "Relevance of beam-column joint damage and collapse in RC frame assessment", *J. Earthq. Eng.*, **6**(1), 75-100.

Caprili, S., Mattei, F., Gigliotti, R. and Salvatore, W. (2018), "Modified cyclic steel law including bond-slip for analysis of RC structures with plain bars", *Earthq. Struct.*, **14**(3), 187-201. https://doi.org/10.12989/eas.2018.14.3.187.

Celik, O.C. and Ellingwood, B.R. (2008), "Modelling beam-column joints in fragility assessment of gravity load designed reinforced concrete frames", *J. Earthq. Eng.*, **12**(3), 357-381. https://doi.org/10.1080/13632460701457215.

Deierlein, G.G., Reinhorn, AM. and Willford, M.R. (2010), "Nonlinear structural analysis for seismic design", NEHRP Seismic Design Technical Brief No. 4, produced by the NEHRP Consultants Joint Venture, a partnership of the Applied Technology Council and the Consortium of Universities for Research in Earthquake Engineering, for the National Institute of Standards and Technology, Gaithersburg, MD, NIST GCR 10-917-5.

Elnashai, A.S. and Di-Sarno, L. (2008), *Fundamentals of Earthquake Engineering*, A John Wiley & Sons, Ltd., West Sussex, UK.

Erdil, B. (2016), "Why RC buildings failed in the 2011 Van, Turkey, earthquakes: construction versus design practices", *J. Perform. Constr. Facil.*, **31**(3), 04016110.

https://doi.org/10.1061/(ASCE)CF.1943-5509.0000980

Fan, G., Wang, D. and Jia, J. (2018), "Improvement, analytical verification and application of RC frame beam-column joint models", *Earthq. Struct.*, **14**(3), 273-283. https://doi.org/10.12989/eas.2018.14.3.273.

Filippou F.C. and Fenves G.L. (2004), "Methods of analysis for earthquake-resistant structures", Chapter 6 in Earthquake Engineering-From Engineering Seismology to Performance-Based Engineering, Eds. Y. Bozorgnia and V.V. Bertero, Cambridge University Press, Cambridge, United Kingdom.

Fragiadakis, M. and Papadrakakis, M. (2008), "Modeling, analysis and reliability of seismically excited structures: computational issues", *Int. J. Comput. Meth.*, **5**(4), 483-511. https://doi.org/10.1142/S0219876208001674.

Inel, M. and Meral, E. (2016), "Seismic performance of RC buildings subjected to past earthquakes in Turkey", *Earthq. Struct.*, **11**(3), 483-503. http://dx.doi.org/10.12989/eas.2016.11.3.483.

Kappos, A.J. (1991), "Analytical prediction of the collapse earthquake for reinforced concrete buildings: suggested methodology", *Earthq. Eng. Struct. Dyn.*, **20**, 167-176. https://doi.org/10.1002/eqe.4290200206.

Kim, J. and LaFave, M. (2012), "A simplified approach to joint shear behavior prediction of RC beam-column connections", *Earthq. Spectra*, **28**(3), 1071-1096. https://doi.org/10.1193/1.4000064.

Lima, C., Martinelli, E., Macorini, L. and Izzuddin, B.A. (2017), "Modelling beam-to-column joints in seismic analysis of RC frames", *Earthq. Struct.*, **12**(1), 119-133. https://doi.org/10.12989/eas.2017.12.1.119.

Lowes, L.N. and Altoontash, A. (2003), "Modeling reinforced-concrete beam-column joints subjected to cyclic loading", *ASCE J. Struct. Eng.*, **129**(12), 1686-1697. https://doi.org/10.1061/(ASCE)0733-9445(2003)129:12(1686).

Neuenhofer, A. and Filippou F.C. (1997), "Evaluation of nonlinear frame finite-element models", *J. Struct. Eng.*, ASCE, **123**(7), 958-966. https://doi.org/10.1061/(ASCE)0733-9445(1997)123:7(958).

Newmark, N.M. and Hall, W. J., (1982), "Earthquake spectra and design", Earthquake Engineering Research Institute, Oakland, CA.

Pampanin, S., Calvi, GM. and Moratti, M. (2002), "Seismic behavior of R.C. beam-column joints designed for gravity only", *Proceedings of the 12th European Conference on Earthquake Engineering*, Paper No. 726.

Paulay and Priestley (1992), *Seismic Design of Reinforced Concrete and Masonry Buildings*, John Wiley & Sons, Inc., NY, USA.

Priestley, M.J.N. (1997), "Displacement-based seismic assessment of reinforced concrete buildings", *J. Earthq. Eng.*, **1**(1), 157-192.

Quintana-Gallo, P., Pampanin, S., Carr, A.J. and Bonelli, P. (2010), "Shake table tests of under designed RC frames for the seismic retrofit of buildings-design and similitude requirements of the benchmark specimen", *Proceedings of the New Zealand Society of Earthquake Engineering*, Paper No. 39.

Rashid, M. and Ahmad, N. (2017), "Economic losses due to earthquake-induced structural damages in RC SMRF structures", *Cogent Eng.*, **4**(1), 1-15.

Rizwan, M., Ahmad, N. and Khan, A.N. (2018), "Seismic performance of compliant and noncompliant special moment-resisting reinforced concrete frames", *ACI Struct. J.*, **115**(4), 1063-1073.

Rossetto, T. and Peiris, N., (2009), "Observations of damage due to the Kashmir earthquake of October 8, 2005 and study of current seismic provisions for buildings in Pakistan", *Bull. Earthq. Eng.*, **7**(3), 681-699. https://doi.org/10.1007/s10518-009-9118-5.

Ruiz-Pinilla, J.G., Adam, J.M., Perez-Carcel, R., Yuste, J. and Moragues, J.J. (2016), "Learning from RC building structures damaged by the earthquake in Lorca, Spain, in 2011", *Eng. Fail. Anal.*, **68**, 76-86. https://doi.org/10.1016/j.engfailanal.2016.05.013.

SeismoStruct (2016), SeismoStruct-Software: a computer program for static and dynamic nonlinear inelastic analysis of structures. Available from URL: www.seismosoft.com.

Sharma, A., Reddy, G.R. and Vaze, K.K. (2012), "Shake table tests on a non-seismically detailed RC frame structure", *Struct. Eng. Mech.*, **41**(1), 1-24. https://doi.org/10.12989/sem.2012.41.1.001.

Sivaselvan, M. and Reinhorn, A.M. (2001), "Hysteretic models for deteriorating inelastic structures", *J. Eng. Mech.*, ASCE, **126**(6), 633-640. https://doi.org/10.1061/(ASCE)0733-9399(2000)126:6(633)

Spacone, E., Ciampi, V. and Filippou, F.C. (1996), "Mixed formulation of nonlinear beam finite element", *Comput. Struct.*, **58**(1), 71-83. https://doi.org/10.1016/0045-7949(95)00103-N.

Vamvatsikos, D. and Cornell, C. (2002), "Incremental dynamic analysis", *Earthq. Eng. Struct. Dyn.*, **31**(3), 491-514. https://doi.org/10.1002/eqe.141.

Youssef, M. and Ghobarah, A. (2001), "Modelling of RC beam-column joints and structural walls", *J. Earthq. Eng.*, **5**(1), 93-111.

CC